# Clogging Evaluation of Porous Asphalt Pavement Using Ground-Penetrating Radar

## ABSTRACT

Clogging reduces the porosity of porous asphalt (PA) pavement, which would jeopardize its permeability, noise absorption, and skid resistance. Existing evaluating methods use in-situ cores that damage the pavement with limited coverage. This study explored the feasibility of evaluating PA pavement clogging using ground-penetrating radar (GPR). Laboratory tests were performed on porous asphalt (PA) slabs under various clogging degrees. The effect of antenna type and moisture on clogging evaluation were investigated. The performances of two clogging indicators were examined, including the bulk dielectric constant obtained using the time-of-flight method and time-frequency spectrograms using the short-time Fourier transform (STFT). Effectiveness of GPR-based clogging evaluation was validated by permeability tests. Results show that both indicators could effectively evaluate clogging in PA pavement. The effectivenesses of proposed indicators were verified through permeability tests. GPR surveys are suggested 72 hours after rainfall in sunny days using 2 GHz air-coupled antennas.

**Keywords：** Porous asphalt pavement; Clogging; Ground-penetrating radar; Dielectric constant; Short-time Fourier transform.

## 1. INTRODUCTION

Porous asphalt (PA) is an open-graded asphalt mixture with high air void content (15%- 25%) [1, 2], which may provide good permeability, strong skid resistance, and low tire-road noise [3]. It has been widely used as a surfacing material of pavement to reduce hazardous stormwater runoff and increase driving safety [4]. However, with time, PA pavement is often clogged by particles carried by urban runoff and precipitation [5, 6]. The clogging materials mainly include crushed aggregate, tire wear residues, metal pollutants, dust, soil, and organic debris [7]. Under the dynamic pore pressure induced by vehicular loading and moisture infiltration, particles may fill the interconnected porous channels, which causes clogging [8]. The reduced porosity would jeopardize PA pavement's permeability and noise-reduction performances [9]. Hence, routine inspection of clogging degree is essential for PA pavement maintenance and rehabilitation purposes [10].

PA pavement clogging can usually be cleaned with a depth up to 10-30 mm by municipal utility equipment such as vacuum hoses, vacuum street sweepers, and regenerative air sweepers [10]. Functions of PA pavement can be partially recovered through proper maintenance procedures. However, the clogging particles are progressively distributed within the pore structure of PA pavement, which is difficult to be detected by visual inspection [11, 12]. Some existing clogging evaluation methods measure the porosity reduction and permeability coefficient loss using in-situ core samples [13]. The permeability of the samples measured by constant-head-based permeability tests is used to assess the clogging degree [14]. X-ray tomography could be applied to capture the distribution of clogging particles in the pore structure along depth [15]. A high correlation was found between the permeability and clogging degree [16, 17]. However, these methods are indirect measurements of the clogging degree. Core samples only cover limited areas, and core-drilling damages the pavement.

Ground-penetrating radar (GPR), an electromagnetic (EM) wave-based method, may be used to characterize clogging degree [18, 19]. It has been commonly utilized as an efficient non-destructive tool (NDT) in pavement thickness prediction, density measurement, utility locating, and defects detection [20, 21]. Subsurface conditions that cause EM wave scattering within the porous medium, such as the fouled railroad ballast, where small-sized particles fill in the skeleton structure formed by coarse aggregates [22, 23], can be evaluated using GPR. The frequency domain features were usually utilized due to the limited information obtained from time domain GPR data. The research methods such as the energy attenuation method [24] and time-frequency analysis methods [25, 26] may be employed to characterize PA pavement clogging. For example, the spectrogram obtained using the short-time Fourier transform (STFT) could provide frequency and time information simultaneously [27]. The time axis can be transformed to depth based on the known dielectric constant of a media [22]. This could allow the evaluation of clogging's effect along the depth of pavement structure.

PA pavement clogging evaluation using GPR may be challenging. The GPR signal waveforms for different clogging degrees have not been fully studied in the literature. The appropriate GPR device and specifications should be evaluated for PA pavement clogging detection. Based on EM mixing theory, a PA mixture's dielectric constant relies on each component's dielectric constant and volumetric property [18]. The bulk dielectric constant of the mixture is expected to increase with more signal scattering as the pore structure is gradually filled with clogging particles. The indicators that can be used to characterize clogging degree need to be studied. In addition, the effect of moisture on the detectability of clogging degree should be investigated because moisture has a significant effect on the dielectric property of asphalt mixture.

The main objective of this study is to explore the feasibility of using GPR to detect clogging in PA pavement through controlled lab tests. GPR data were collected from PA slabs with different clogging degrees to analyze the corresponding responses in the GPR signal. The effectivenesses of two clogging indicators were examined, namely, bulk dielectric constant using the time-of-flight method and STFT

spectrogram using time-frequency analysis. The effects of GPR antenna type and moisture content on the clogging detection accuracy were analyzed. The permeabilities of PA mixtures under different clogging degrees were measured to validate the GPR clogging detection results. The proposed method may contribute to the direct and non-destructive detection of PA pavement clogging using GPR. But it is worth noting that "clogging" refers to particle-related clogging in this paper. The deformation-related clogging caused by traffic loading is not within the scope of this study.

## 2. METHODS

### 2.1 Laboratory Investigation

Laboratory tests were performed to explore the effect of clogging degree on the dielectric constant measurement and GPR signal waveform. Asphalt mixture slabs were first manufactured and clogged to different degrees. Then, both GPR measurements and permeability tests were conducted.

#### *2.1.1 Polymer Modified Friction Course (PMFC) Slabs*

The polymer modified friction course (PMFC) mixture, which is an open-graded PA widely used in Hong Kong, was used to prepare asphalt slabs using a rolling wheel compactor. The sizes were 30cm × 30cm × 5 cm. The aggregate was granite from Guangdong province, China. PG76-16 polymer-modified asphalt binder was used with a content of 4.5% by the mass of the mixture. The mixture gradation is shown in Figure 1. The design air void content was 20%. The air void content after slab manufacturing is calculated by using the following equation [28]:

$$AV\% = \left(\frac{G_{mm}-G_{mb}}{G_{mm}}\right) \times 100 \quad (1)$$

where $AV\%$ is the air void content in percent; and $G_{mm}$ and $G_{mb}$ are the theoretical maximum specific gravity and the bulk specific gravity of the PMFC mixture, respectively.

$G_{mm}$ is determined by using the weighing in water method of the loose mixture, as calculated by the following equation [29]:

$$G_{mm} = \frac{A}{A-C} \quad (2)$$

where $A$ is the sample mass in air; and $C$ is the mass of water displaced by the sample.

$G_{mb}$ is calculated by using the volume method. The average $AV\%$ of all slabs is 19.8%, with a standard deviation of 0.004.

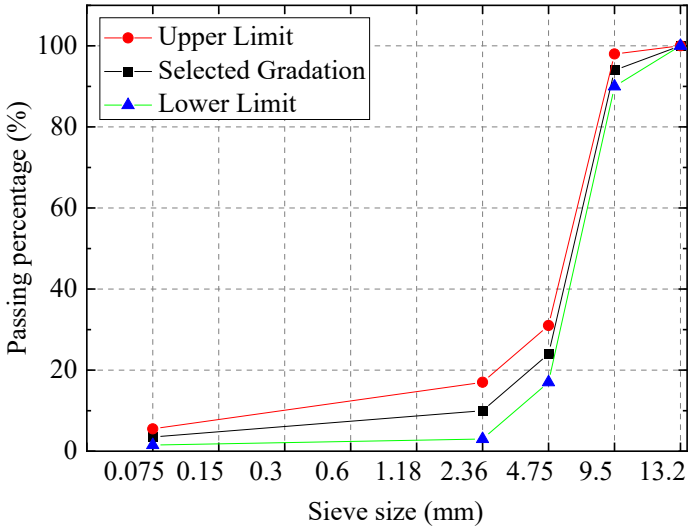


Figure 1. Aggregate gradation of the PMFC mixture

*2.1.2 Clogging Material*

Fine granite particles with a size of 0.075-2.36 mm were prepared as clogging material in this study. This size has been proved as the main component in pavement runoff sediments causing clogging [17]. Particles larger than 2.36 mm could barely fill the interconnected pore structures, and those less than 0.075 mm may be flushed out of the slabs through interconnected voids [30]. The mass of clogging solid on each slab was determined from a study on rainfall pollutant evaluation. A runoff solution with the known total suspended solid (TSS) concentrations of 550 mg/L was selected from a nationwide urban runoff program (NURP) in California, USA [31]. The runoff volume was assumed to be 200 L [11]. Hence, the total clogging particle mass on each slab was 110 g. The slabs were clogged by fine particles at four percentage levels of the total mass (25%, 50%, 75%, and 100%) to evaluate GPR's detectability under different clogging degrees. It should be noted that the effect of the particle size distribution (PSD) is not considered in this study.

*2.1.3 GPR Data Acquisition*

A ground-coupled 2 GHz palm antenna system and an air-coupled 2 GHz horn antenna system, both manufactured by Geophysical Survey Systems, Inc. (GSSI), were used in the laboratory tests. The palm antenna system was connected to a portable control unit (SIR 4000) and was hand-held by operators during data acquisition. The horn antenna system was connected to a multi-channel control unit (SIR 30) and was mounted on a customized cart. GPR data s were collected in the static time mode for both antenna systems, i.e., certain numbers of signal traces were collected in unit time. The time window of a single GPR A-scan was 12 ns. The sampling rate of each signal was 1,024 to ensure sufficient time-domain resolution for time-frequency analysis (0.0117 ns/sample). During GPR measurements, nine PMFC slabs were assembled as a large slab of 90 cm×90 cm×5 cm. For the palm antenna system, it was tightly attached to the slab during data collection. Individual data were obtained from each slab due to the limited antenna footprint. For the horn antenna system, the antenna-surface height was kept constant at 40 ± 0.2 cm to avoid signal drifting between GPR measurements. Under this antenna-surface height, the antenna footprint is within the formed square, as shown in Figure 2. The incomplete reflection from the edge, i.e., edge effect, can be assumed negligible under this configuration [32]. The orientation of each slab remained unchanged before and after clogging to eliminate the effect of clogging variation at different directions. Figure 2 illustrates the settings for GPR data collection.

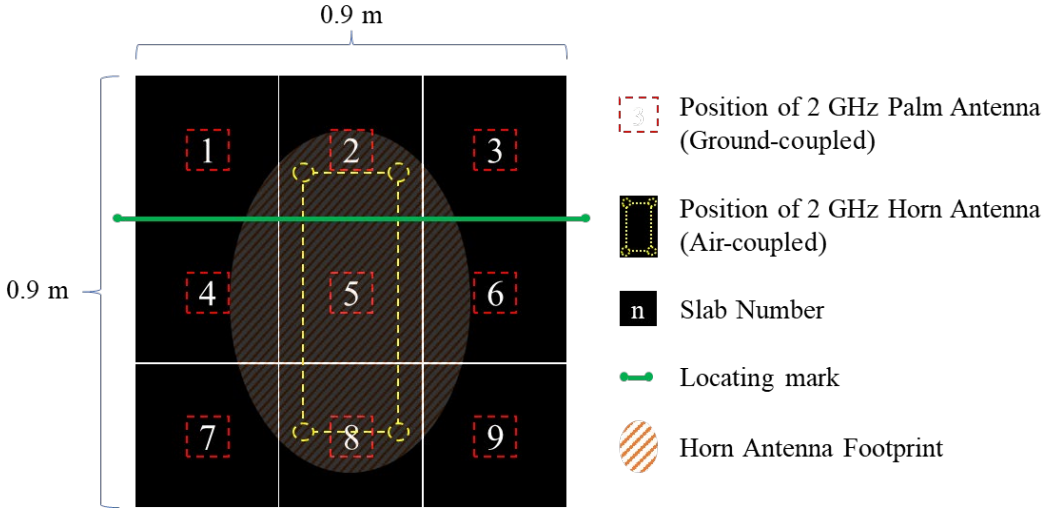


Figure 2. Settings for GPR data collection

*2.1.4 Clogging and GPR Testing Procedure*

Indoor clogging and GPR tests were implemented in the lab-controlled environment. A tarp was placed underneath the slabs to provide waterproofing and locate slabs during the test, as shown in Figure 3 (a).

GPR measurements using both palm and horn antenna were conducted on the assembled slabs, as shown in Figure 3 (b) and (c). GPR data from the clean slabs was collected as the benchmark. During the clogging process (Figure 3 (d)-(f)), the clogging materials were sprinkled on the interior of the slab. A brush was used to distribute the particles over the slab surface evenly. The particles were sprayed for 15 minutes on each slab. The particles remained on the slab surface may only affect the surface reflection amplitude in GPR signals. Hence, they were not removed because the surface reflection amplitude was not used in signal processing. During the spraying process, interior sprinkled particles will be re-distributed towards the whole slab by the dynamic pore pressure caused by the spraying operation. The residue sprayed outside the slab will be collected from the bottom of the basin and re-flushed. After clogging, the slabs were positioned still for 15 minutes, then the bottom of each slab was wiped with a dry towel. This ensures no water seepage exists in the slabs during GPR measurements. After GPR measurements, the slabs were stored without stacking until interior moisture completely evaporated at room temperature. GPR data were collected 1 hour, 24 hours, 48 hours, and 72 hours after each clogging operation to investigate the effect of internal moisture. The clogging materials were at four levels (25%, 50%, 75%, and 100%) of the total mass of fine particles.

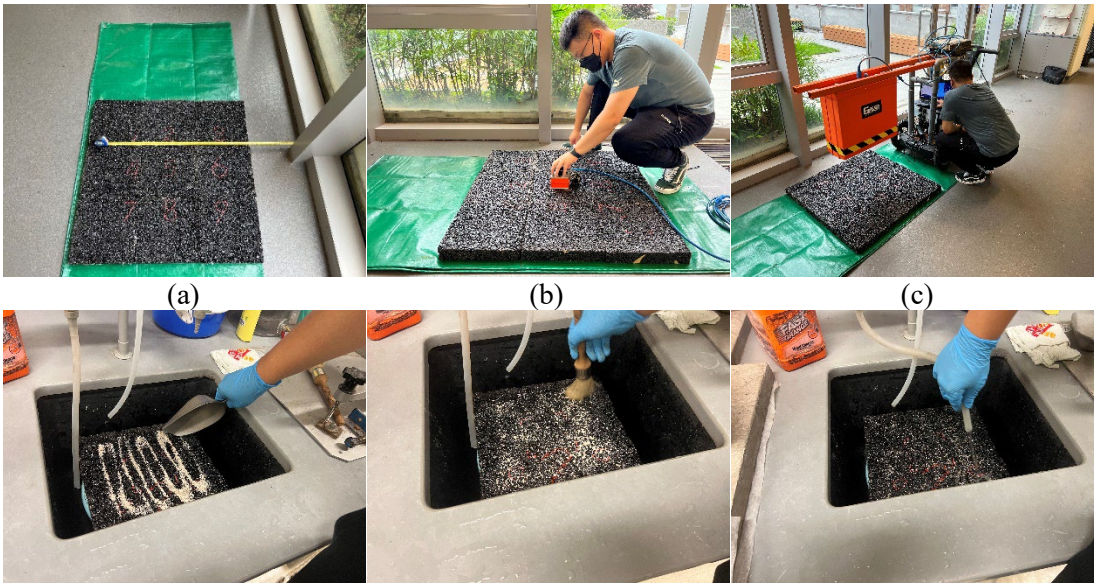

(a) (b) (c)

(d) (e) (f)

Figure 3. Laboratory test procedure: (a) locating; (b) palm antenna measurement; (c) horn antenna measurement; (d) sprinkling; (e) brushing; (f) spraying.

*2.1.5 Permeability Test*

Three PMFC slabs were cored to prepare Marshall specimens with a diameter of 96mm for permeability test, as shown in Figure 4 (a). A custom-designed constant-head permeability apparatus was utilized according to BS EN 12697-19:2012, as shown in Figure 4 (b) [33]. The lateral surface of the cylinder specimen and the gap between the specimen and the apparatus were tightly sealed. Three measurements were conducted and averaged for each specimen. The vertical permeability of PA mixture was calculated by using the following equation:

$$K_V = \frac{Q_v L}{AHt} \tag{3}$$

where $K_V$ is the vertical permeability of PA specimen in centimeters per second (cm/s); $Q_v$ is the vertical flow in $t$ seconds in milliliter (ml); $L$ is the thickness of the specimen in centimeters (cm); $A$ is the area of the upper surface of the specimen in square centimeters ($cm^2$); $H$ is the waterhead in centimeters (cm); and $t$ is the measured time interval in second (s).

During the permeability test, PA Marshall specimens were clogged at four levels of total mass as well (25%, 50%, 75%, and 100%). The total clogging particle mass of each Marshall specimen was 8.85 g, which was calculated by using Equation 4:

$$M_{Marshall} = M_{Slab} \cdot \frac{A_{Marshall}}{A_{Slab}} \quad (4)$$

where $M_{Marshall}$ is the total mass of particles that were used to clog the Marshall specimens in the permeability test in grams (g); $M_{Slab}$ is the total mass of particles that were used to clog the PA slabs in GPR measurements in grams (g); $A_{Marshall}$ is the area of the upper surface of Marshall specimen that equals to 72.38 $cm^2$; and $A_{Slab}$ is the area of the upper surface of PA slab that equals to 900 square $cm^2$.

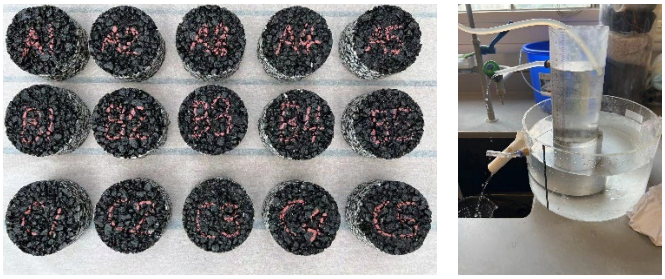

(a) (b)

Figure 4. Permeability test: (a) drilled PA Marshall mixture; (b) apparatus

## 2.2 GPR Data Interpretation

### *2.2.1 Dielectric Constant Calculation*

Both the reflection amplitude method and the time-of-flight method can be used to calculate the dielectric constant of the asphalt pavement layer. For the reflection amplitude method, the amplitude of the reflective signal from the pavement surface and a perfect reflector (e.g., a copper plate) are used in the dielectric constant estimation [34]. It has been widely applied in pavement layer thickness prediction and in-situ density measurements [35,36]. However, this method assumes the homogeneity of the dielectric constant distribution from layer top to bottom, which may cause errors in existing pavement [37]. Meanwhile, the surface or internal moisture would significantly affect the surface reflection amplitude, then the dielectric constant estimation accuracy [37]. Hence, the surface reflection method is not appropriate for evaluating PA pavement clogging. The time-of-flight method calculates the dielectric constant by using the propagation time of EM waves within the pavement layer. It can be obtained by manual observation of the GPR A-scan signal [19]. Then, the bulk dielectric constant of PA pavement could be estimated when the layer thickness is known using Equation 5. This method considers the inhomogeneity of pavement layer and can track the material property changes [38]. Hence, in this study, the time-of-flight method was employed on raw GPR data from both antennas to estimate the bulk dielectric constant of PMFC mixture.

$$\varepsilon_r = \left(\frac{ct}{2d}\right)^2 \quad (5)$$

where $\varepsilon_r$ is the bulk dielectric constant of the PA mixture; $c$ is the speed of light ($3\times10^8$ m/s); $t$ is the two-way travel time (s); and $d$ is the thickness of PA slab, equal 5 cm in this case.

### *2.2.2 Short-Time Fourier Transform*

The Short-Time Fourier Transform is a time-frequency representation (TFR) method that can provide both time and frequency information of GPR signal [27]. The STFT of a signal $x(\tau)$ is represented by Equation 6:

$$\mathrm{STFT}(t, \Omega) = \int_{\tau}[x(\tau)\cdot w(\tau - t)] \cdot e^{-j\Omega t}\, d\tau \quad (6)$$

where $x(\tau)$ is the reflected GPR signal; $t$ is the time variable; $\tau$ is the time variable of the reflected GPR signal; $\Omega$ is the radial frequency variable; $w(\tau-t)$ is the window function, which is selected as Hamming window [23]; and STFT is the frequency energy at time $t$ and frequency $\Omega$.

The spectrogram of STFT on GPR signals was analyzed to capture time-frequency clogging features along the depth. In STFT, time and frequency resolutions cannot be achieved simultaneously. Increasing the resolution in the time domain jeopardizes that in the frequency domain, and vice versa. Hence, different window lengths were applied to evaluate the clogging effect on GPR data.

## 3. RESULTS & DISCUSSION

### 3.1 Effect of Gaps between Slabs

Due to the assembling operation, the large PMFC slab has tiny gaps between slabs with a maximum width of 2 mm. These gaps may generate reflections affecting signals that are used for clogging evaluation. Their effect can be neglected when the ground-coupled antenna is used because the footprint is within the single slab. However, the gaps between slabs may camouflage the clogging evidence in the air-coupled antenna signals due to the wide-angle radiation pattern of this antenna type [39]. The corresponding GPR B-scan was acquired, as shown in Figure 5. An inconsistency of stratified reflection at the square surface occurred in the gray-scale B-scan image, representing the position of the slab edge. The surface and bottom positions of the slabs were captured as marked in the yellow rectangular region in Figure 5. Hyperbolic reflection feature, which indicates cracking in this study [40], was not found in B-scan at assembled slab square position. This indicates that the gaps between slabs in laboratory investigation have negligible effect on clogging evaluation using the air-coupled GPR data.

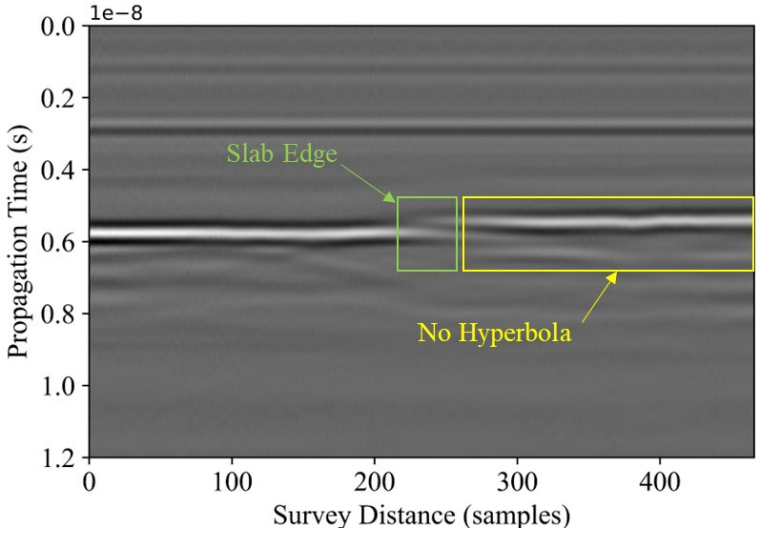


Figure 5. B-scan image of assembled PMFC slabs using air-coupled horn antenna.

### 3.2 Effect of Antenna Type

Figure 6 and **7** shows the GPR A-scans of clean PMFC slabs using the air-coupled and ground-coupled antennas, respectively. During GPR data acquisition, a copper plate was placed at the PA slab surface and bottom sides. This could help locate the reflection locations from both sides of the PA slab for two-way travel time (TWTT) identification due to the strong reflection waveform from the copper plate. In the air-coupled GPR data, a direct coupling pulse from transmitter to receiver without going through the slab occurs at 3 ns, as shown in Figure 6. The amplitude of this direct coupling is lower than those from PA slab reflection signal. This is because both transmitter and receiver inside the antenna were shielded from each other to avoid significantly large amplitude from direct coupling. The surface and bottom reflections of the slabs can be identified at 5.42 ns and 6.14 ns, respectively. TWTT for electromagnetic wave propagation within the slab can be manually extracted and estimated. Although the bottom reflection is

partially coupled with the surface reflection, its position can be located by visual inspection [36]. Hence, the dielectric constant of the PMFC mixture can be obtained precisely using the air-coupled GPR data.

In the ground-coupled GPR data, the coupling pulse is removed automatically by SIR 4000 control unit during post-processing. The surface reflection was captured at 0.58 ns, as shown in Figure 7. However, the system configuration of ground-coupled palm antenna is different from the air-coupled horn antenna. It is challenging to identify the bottom reflection directly from GPR A-scan. In this study, the bottom reflection was estimated (red line in Figure 7) by using time delay in the air-coupled GPR data as a reference. This indicates the deficiency of the ground-coupled palm GPR when it is applied without the air-coupled antenna to characterize clogging in PA pavement. It should be noted that the lab tests were conducted on the floor of a laboratory building. Signals after 1.31 ns in the ground-coupled data represented subsurface reflection between the floor decks, which is not of interest in this study. In real pavement structures, PA pavement serves as the functional wearing course. Signals after its bottom reflection will come from the underlying pavement layers, including surface layers, base layers, and the foundation, which do not affect the signal analysis for clogging detection. During field implementations, the air-coupled antenna is recommended to locate the potential clogging area. If traffic closure is allowed, ground-coupled palm GPR could be employed as a compensation at the identified areas. The ground-coupled antenna could provide a higher resolution clogging map than the air-coupled one due to its smaller EM radiation footprint.

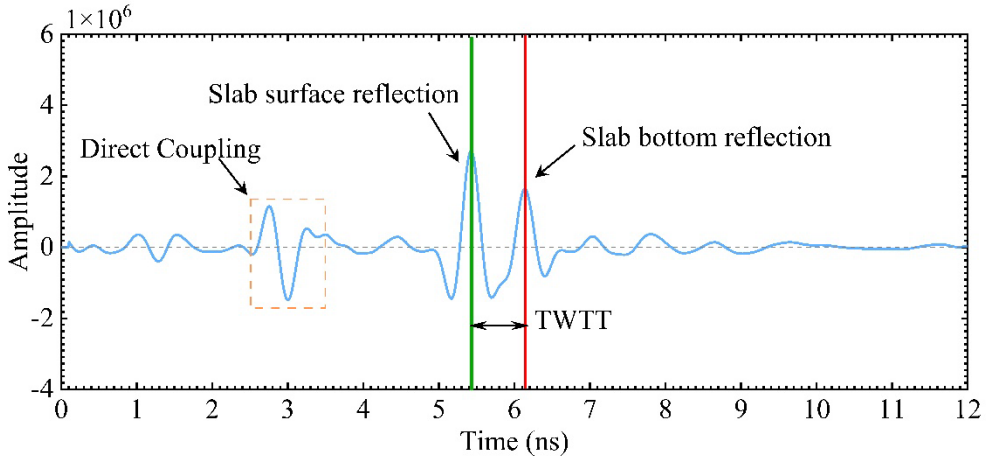


Figure 6. A-scan waveform of clean (benchmark) PMFC slabs using air-coupled horn antenna.

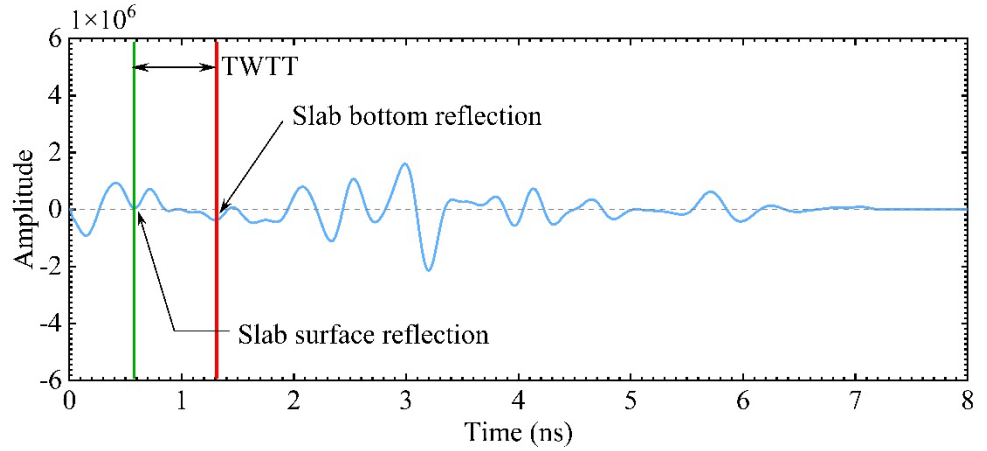


Figure 7. A-scan waveform of clean (benchmark) PMFC slabs using ground-coupled palm antenna.

### 3.3 Effect of Moisture Content

The existence of moisture increases the bulk dielectric constant of the media due to its high electric impedance, which causes difficulty in clogging evaluation using GPR. Figures 8 and 9 show the GPR signals from slabs with 25% and 50% clogging material degrees over time using air-coupled and ground-coupled antennas, respectively. For both antennas, the surface reflection amplitude reaches the maximum after the clogging operation, and gradually recovers to its origin as moisture keeps evaporating. However, the bottom reflection may not be identified at this stage. This is expected because of the conductivity of water, which absorbs electromagnetic wave energy and blurs pavement information from the signal [22]. From 48 to 72 hours after clogging, evident bottom reflection could be observed with a stable position. Results suggest that clogging evaluation using GPR should be performed at least 72 hours after rainfall or precipitation events on sunny days to eliminate moisture's effect. Note that the moisture could be trapped in the PA pavement for an extended period during the rainy season. Therefore, GPR is not recommended for clogging detection during the rainy season. In this paper, GPR data at 72 hours was used as dry condition to ensure dielectric constant estimation accuracy.

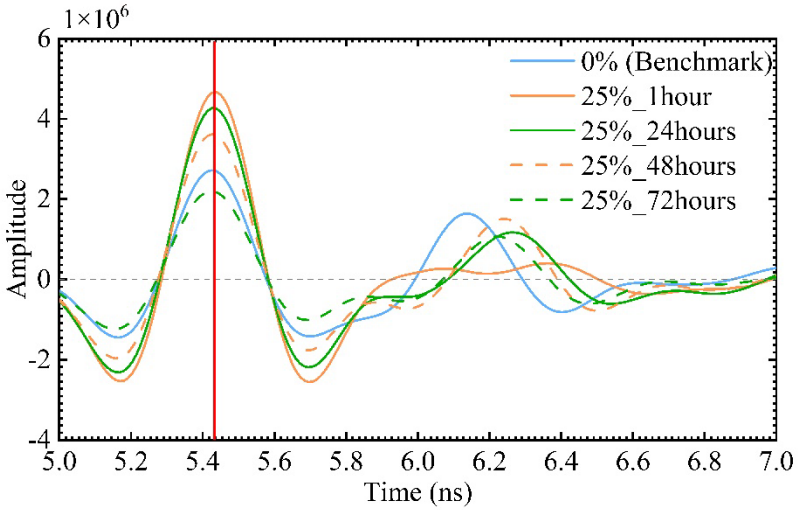


Figure 8. A-scan of 25% clogged PMFC slabs under different moisture contents using air-coupled horn antenna.

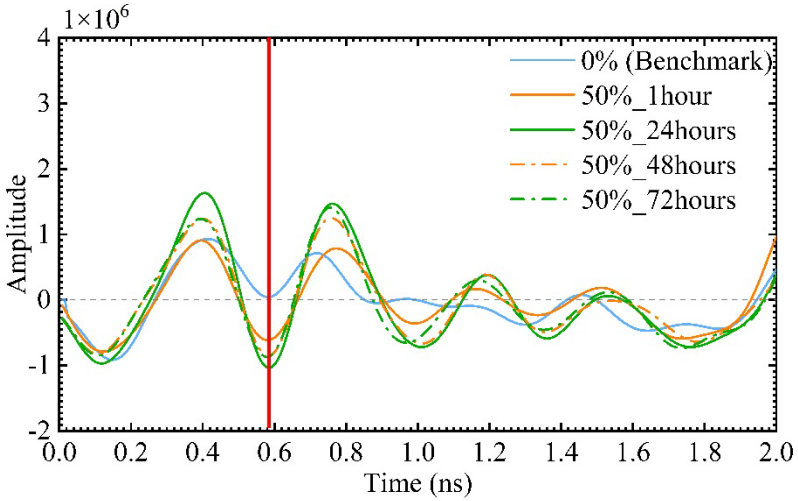


Figure 9. A-scan of 50% clogged PMFC slabs under different moisture contents using ground-coupled palm antenna.

### 3.4 Clogging Evaluation Indicator I: Dielectric Constant

The bulk dielectric constant results using air-coupled and ground-coupled GPR data are shown in Figure 10 and 11, respectively. Noted that air-coupled data was collected from the large slab, composed of 9 small slabs, as a whole. Therefore, there is no error bar in Figure 10. For the clean PMFC mixture, the bulk dielectric constants were 4.64 and 4.88 using air-/ground-coupled GPR data, respectively. For ground-coupled GPR data, the average dielectric constant from 9 slabs was calculated under each clogging degree with a maximum coefficient of variation (CV) of 7.4%. This demonstrates the consistency between measurements and the reliability using GPR to evaluate PA pavement clogging. The bulk dielectric constants from both antenna types increase as the clogging degree increases, which is expected based on EM mixing theory. No further increment was shown with respect to the bulk dielectric constant after 75% clogging material was sprayed. This phenomenon is consistent with the field observation that fine particles accumulated and remained on the slab's surface, representing that the pore structure was fully clogged. This validates the advantage of the time-of-flight method over reflection amplitude method because the PA pavement surface condition or any left debris does not affect the bulk dielectric constant calculation. However, it is note worthing that the dielectric constant calculation accuracy relies on precise estimation of propagation time of EM wave within the porous layer.

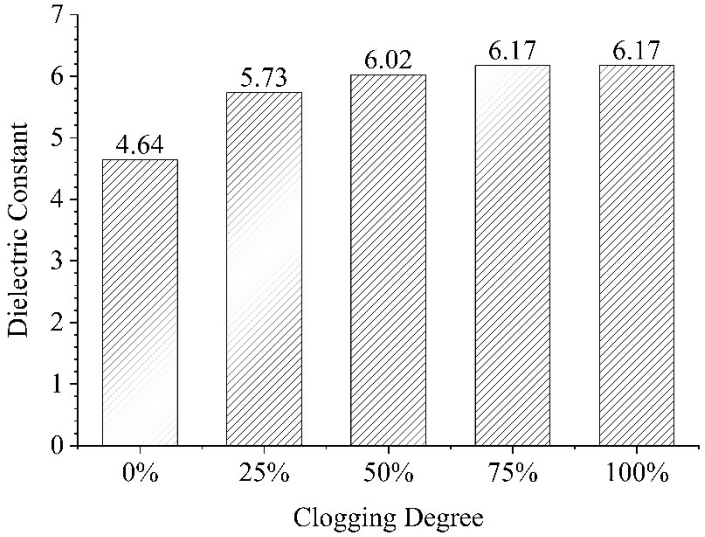


Figure 10. Dielectric constant of dry PMFC slabs under different clogging degrees using air-coupled horn antenna.

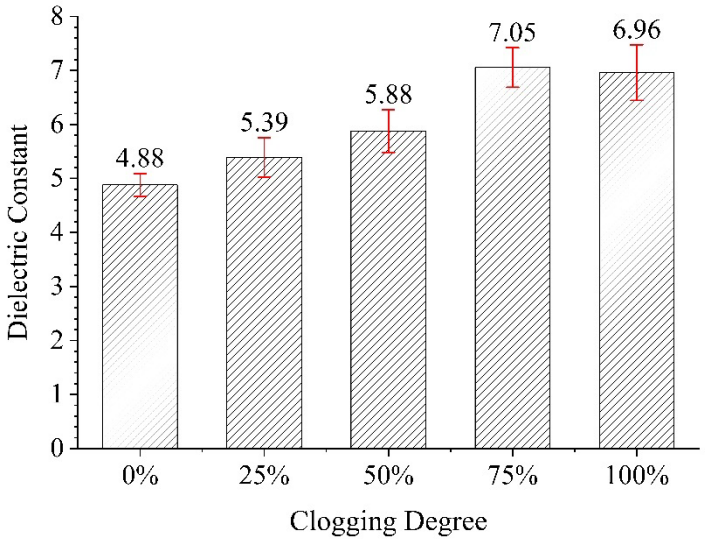


Figure 11. Dielectric constant of dry PMFC slabs under different clogging degrees using ground-coupled palm antenna.

### 3.5 Clogging Evaluation Indicator II: STFT Spectrogram

In the STFT spectrograms, a brighter color indicates more frequency energy accumulations. Figure 12 shows STFT results from clean, 25%, 50%, and 75% clogged slabs with a window length of 8 samples. From Figure 12 (a), the energy gradually attenuates along the depth within the clean PMFC slabs, which is consistent to findings in previous studies [22, 23]. The position of slab surface and bottom could also be detected by strong energy concentration from the spectrogram. In addition, this window length allows identification of surface and bottom reflection positions, leading to accurate layer thickness estimation compared to that using the time-of-flight method.

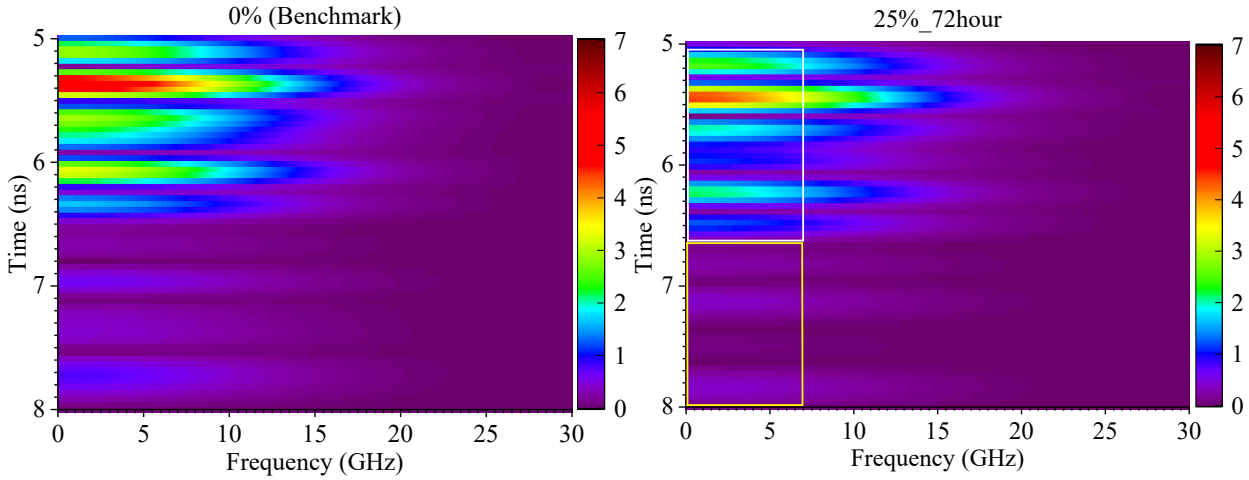

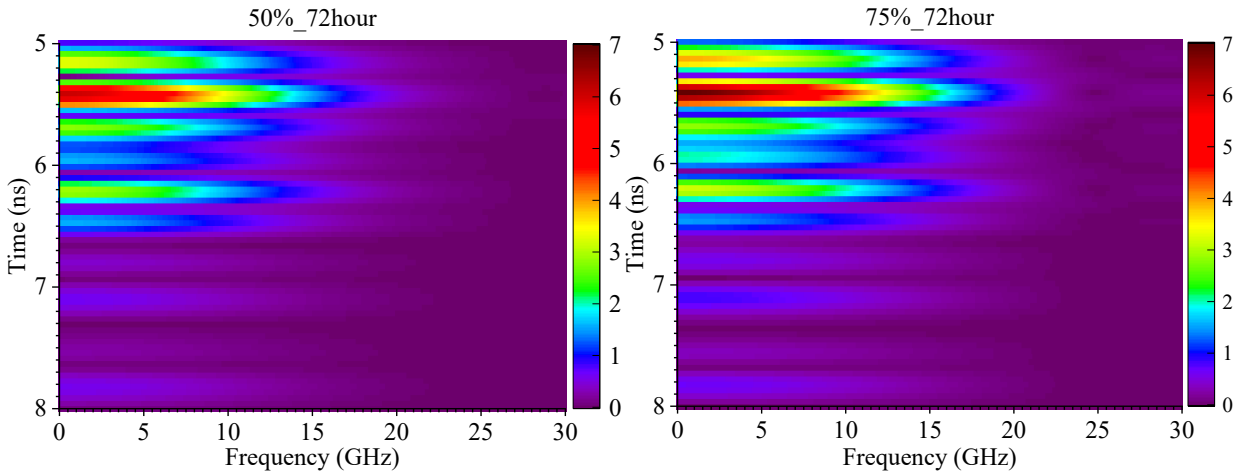


Figure 12. Energy drop in STFT of air-coupled GPR data under different clogging degrees with a window length of 8 samples: (a) 0%; (b) 25%; (c) 50%; (d) 75%

As the sprayed clogging material increased from 0% (clean) to 25%, two significant energy drops were observed in two regions by comparing the STFT spectrogram in Figure 12 (a) and (b). The first energy drop occurs within the slabs. This may be caused by fine clogging particles' occupation in the pore structure as scatterers. The second energy drop occurs beneath the slabs. This indicates that clogging in the porous asphalt layer causes energy attenuation not only within the clogging depth but also adjacent region beneath it. These two energy drops can be quantitively evaluated by calculating the energy sum from STFT spectrogram, as shown in Figure 13. In fact, energy decreases of 24.02% and 49.96% were observed in these two regions. This may help GPR data interpretation by distinguishing clogging from other pavement distresses. However, as the sprayed clogging material continue to increase at 50% and 75%, as shown in Figure 12 (c) and (d), less evident changes were observed with respect to frequency energy. This demonstrates that STFT spectrograms of GPR data with a narrow window length can detect clogging when PA pavement is not fully clogged. In field applications, PA pavement is rarely in a fully clogged state due to the routine cleaning conducted by relevant highway agencies and/or the cleaning effects from moving vehicles. Therefore, the effectiveness of proposed STFT spectrograms as clogging indicators is guaranteed.

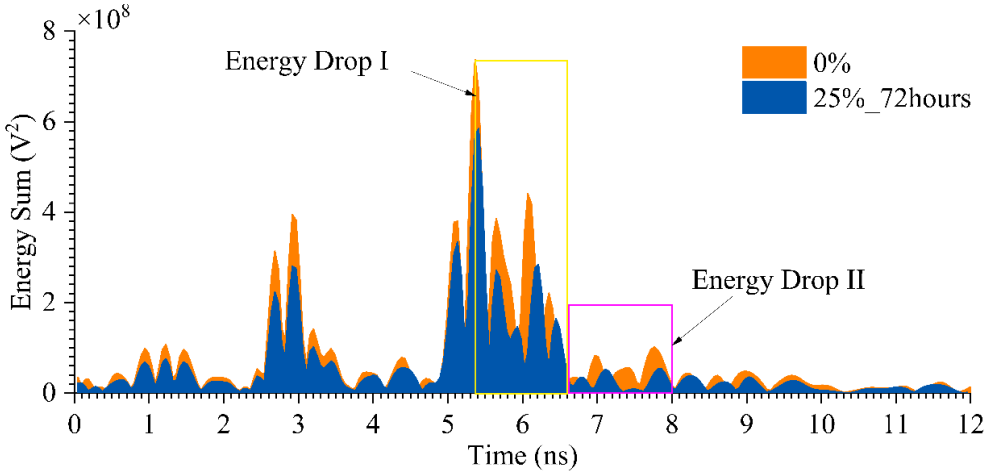


Figure 13. Energy sum of clean and 25% clogged PA mixture STFT spectrogram after 72 Hours

Figure 14 shows the STFT spectrogram of clean and 25% clogged GPR data with different window lengths. With a moderate window length of 32 samples, as shown in Figure 14 (a) and (b), a more significant energy attenuation could be observed within and beneath the slabs, compared with Figure 12 (a) and (b). This validates the effectiveness of using GPR spectrograms as a clogging evaluation indicator. However, it is challenging to identify the location of slab surface and bottom with such moderate window length due to the uncertainty principle [27]. As the window length reaches to 64 samples, frequency information becomes clearer at the cost of layer thickness prediction accuracy, as shown in Figure 14 (c) and (d). Thus, a balanced procedure considering both energy attenuation and slab positioning is suggested using the STFT spectrograms to characterize PA pavement clogging. Moderate window length STFT can be firstly applied to evaluate the existence of PA pavement clogging. Then, narrow window length STFT can be used to accurately provide layer thickness profile. It is worth noting that a sampling frequency of 1,024 points per A-scan is not applicable during field tests using vehicle-mounted GPR system without a traffic closure. One possible solution is performing upsampling (interpolation) operation on GPR raw data, which may increase both time and frequency domain resolutions in STFT spectrogram.

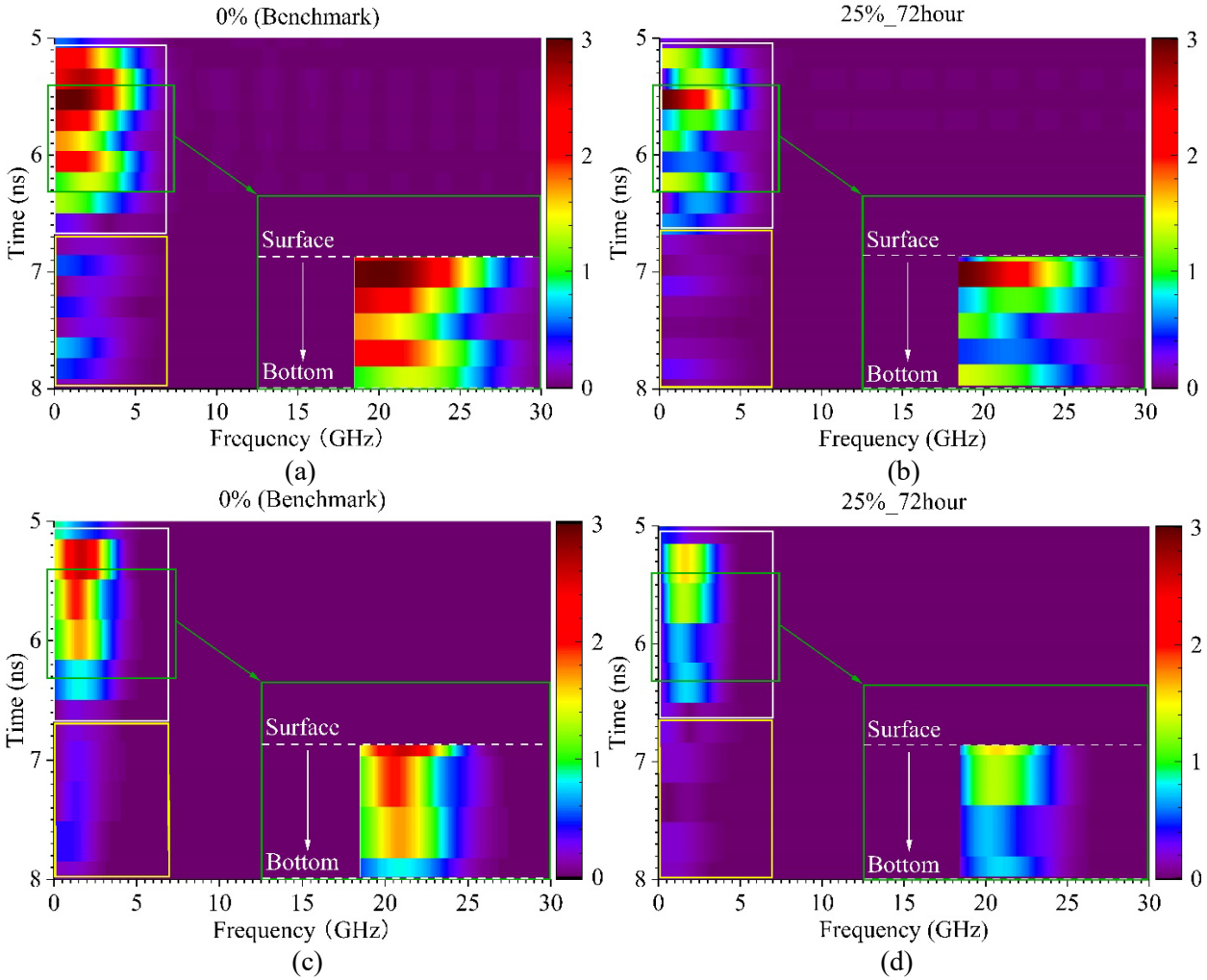


Figure 14. Effect of window length on STFT spectrogram: (a) and (b) are clean and 25% clogged data with a window length of 32 samples, respectively; (c) and (d) are clean and 25% clogged data with a window length of 64 samples, respectively.

In summary, both the bulk dielectric constant using the time-of-flight method and energy variation using the STFT spectrogram show their potential to characterize clogging in PA pavement. The dielectric

constant is a widely accepted estimator in GPR applications, which could be obtained for near real-time evaluation of clogging degrees. However, it can be affected by other factors such as density variations caused by traffic loadings, and asphalt degradation. The STFT spectrogram provides information in both the time and frequency domains, making it more robust than the dielectric constant in clogging evaluation. However, the post-processing could be time-consuming, and a proper window length is suggested to reach optimal performance. It is recommended to use both indicators for a comprehensive evaluation of PA pavement clogging. The proposed GPR-based clogging evaluation method is suggested to be performed following required QA/QC procedures or after high precipitation in the tested region due to possible traffic closure required by the tests.

### 3.6 Permeability of PA mixture

Figure 15 depicts the relationship between PA mixture permeability and clogging degree. Average permeability decreases from 0.266 cm/s to 0.222 cm/s as 25% clogging material was sprayed on clean PA specimens. As the clogging degree becomes severer, permeability continues to drop until 0.16 cm/s at 100% clogging status. The permeable performance decreases by 39.8% compared with that without clogging. The CV of the permeability measurements decreases as the clogging degree increases, indicating a steady flow at low permeability. Combined with the visual inspection of the mixture surface condition, it could be found that no particles appear at the mixture surface until 75% clogging material was sprayed on the specimens. At this stage, the decrease in permeability was mainly caused by clogging. After this threshold, particles were found to remain at the mixture surface, which represents that the interconnected pore structure may be fully clogged. Further permeability decrease is caused by surface accumulation of fine particles. In addition, visual observations are consistent with GPR-characterized clogging conditions using the two indicators (Figures 10, 11 and 12). The effect of particle accumulation at the specimen surface is negligible to dielectric constant and STFT measurements because it only affects the surface amplitude in A-scan signal.

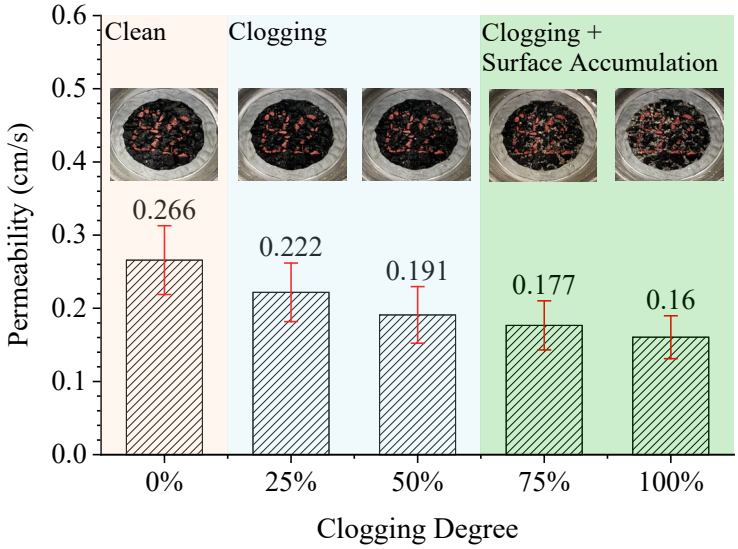


Figure 15. Permeability of PA mixture under different clogging degrees.

The relationship between measured permeability and the predicted dielectric constant of the PMFC mixture is shown in Figure 16. As the permeability decreased from 0.266 cm/s to 0.177 cm/s, the bulk dielectric constant increased accordingly for both air-coupled and ground-coupled antenna data. This is expected because both parameters are significantly affected by inner air void content variations. Although the accumulation of surface residual particles led to further decrements in permeability from 0.177 cm/s to 0.16 cm/s, it did not affect the bulk dielectric constant value. This phenomenon demonstrated the

advantage of using the latter as a reliable clogging indicator, i.e., the insensitivity to surface residues that are out of the scope of the clogging definition. In addition, the correlations are affected by antenna type. For field applications, permeability tests are suggested to be performed at discrete locations in advance as a reference.

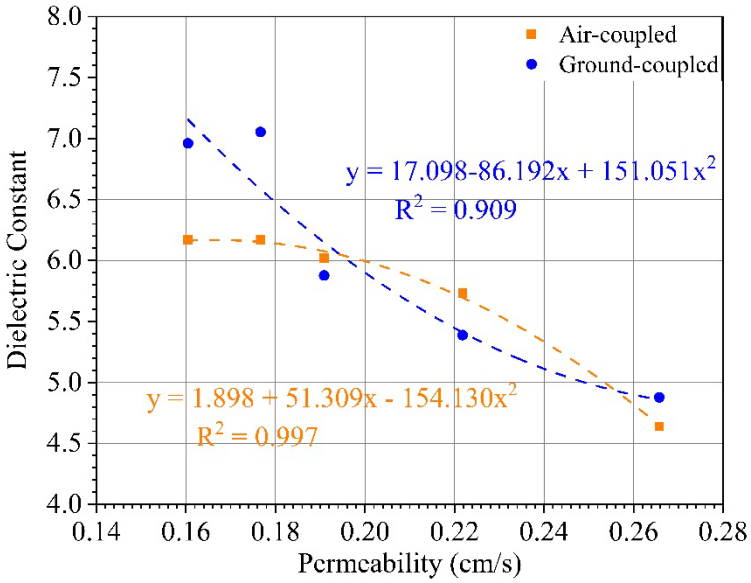


Figure 16. Correlation between permeability and dielectric constant of PMFC mixture under different clogging degrees

## 4. CONCLUSIONS

In this study, the detectability of GPR in evaluating PA pavement clogging was investigated. PMFC slabs with different clogging degrees were manufactured and both GPR surveys and permeability tests were conducted. The effect of antenna type and moisture content were investigated. The performances of two possible clogging evaluation indicators using GPR, namely the bulk dielectric constant of PA mixture using the time-of-flight method and the STFT spectrograms, were evaluated. The effectiveness of using GPR to characterize PA pavement clogging was validated through permeability tests. The main conclusions are drawn as follows:

- The bulk dielectric constant using the time-of-flight method can be used as an effective indicator to characterize clogging degree of PA pavement. A strong linear relationship was found between the bulk dielectric constant and clogging degree, especially when the interconnected pore structure is not fully clogged. The STFT spectrogram of GPR data can be used as an indicator to characterize clogging at minor or moderate clogging degree. Optimal window lengths were required by trials-and-errors until the clogging degree and location information is identified.
- A 2 GHz air-coupled horn antenna is preferred over the ground-coupled palm antenna for clogging evaluation. If traffic closure is permitted, a ground-coupled palm antenna could be used to locate clogging regions as a supplement. It is recommended to perform GPR PA pavement clogging detection on a sunny day at least 72 hours after rainfall. In a raining season with continuous high precipitation, GPR's detectability on clogging is hindered. The proposed method is not suggested for usage due to the effect of long-trapped moisture.
- The bulk dielectric constant of PA pavement correlates well with permeability under different clogging degrees due to their sensitivities to air void content variation. The correlation may be affected by the GPR antenna types. For field applications, permeability tests are suggested for calibration purpose.

The effectiveness of the proposed method and clogging indicators will be further verified through field GPR surveys on PA pavement in future research. The effects of PA mix design, air void content, environmental noise, and pavement cleaning operation will be examined.

## ACKNOWLEDGMENTS

The work described in this paper was partially supported by a grant from the Research Grants Council of the Hong Kong Special Administrative Region, China (PolyU 15209920 for GRF project funded in 2020/21 Exercise).

## REFERENCES

[1] Zhang, Z., A. Sha, X. Liu, B.Luan, J. Gao, W. Jiang, and F. Ma. State-of-the-art of porous asphalt pavement: Experience and considerations of mixture design. *Construction and Building Materials*, Vol. 262, 2020, 119998.

[2] Cooley, L. A., J. W. Brumfield, R. B. Mallick, W. S. Mogawer, M. Partl, L. Poulikakos, and G. Hicks. Construction and maintenance practices for permeable friction courses. *Transportation Research Board*, 2009.

[3] Flintsch, G. W., L. Tang, S. W. Katicha, E. de León Izeppi, H. Viner, A. Dunford, and K. Smith. Splash and spray assessment tool development program. Virginia Tech. Virginia Tech Transportation Institute, 2014.

[4] Wang, D., A. Schacht, Z. Leng, C. Leng, J. Kollmann, and M. Oeser. Effects of material composition on mechanical and acoustic performance of poroelastic road surface (PERS). *Construction and Building Materials*, Vol. 135, 2017, pp. 352-360.

[5] Jacobson, C. R. Identification and quantification of the hydrological impacts of imperviousness in urban catchments: A review. *Journal of environmental management*, Vol. 92, No. 6, 2011, pp. 1438-1448.

[6] Kayhanian, M., D. Anderson, J. T. Harvey, D. Jones, and B. Muhunthan. Permeability measurement and scan imaging to assess clogging of pervious concrete pavements in parking lots. *Journal of Environmental management*, Vol. 95, No. 1, 2012, pp. 114-123.

[7] Dempsey, B. A., and D. M. Swisher. Evaluation of porous pavement and infiltration in Centre County, PA. *In World Water & Environmental Resources Congress 2003*, 2003, pp. 1-11.

[8] Deo, O., M. Sumanasooriya, and N. Neithalath. Permeability reduction in pervious concretes due to clogging: experiments and modeling. *Journal of Materials in Civil Engineering*, Vol. 22, No. 7, 2010, pp. 741-751.

[9] Kia, A., H. S. Wong, and C. R. Cheeseman. Defining clogging potential for permeable concrete. *Journal of environmental management*, Vol. 220, 2018, pp. 44-53.

[10] Sandoval, G. F., A. C. de Moura, E. I. Jussiani, A. C. Andrello, and B. M. Toralles. Proposal of maintenance methodology for pervious concrete (PC) after the phenomenon of clogging. *Construction and Building Materials*, Vol. 248, 2020, pp. 118672.

[11] Coleri, E., M. Kayhanian, J. T. Harvey, K. Yang, and J. M. Boone. Clogging evaluation of open graded friction course pavements tested under rainfall and heavy vehicle simulators. *Journal of environmental management*, Vol. 129, 2013, pp. 164-172.

[12] Zhang, J., R. She, Z. Dai, R. Ming, G. Ma, X. Cui, and L. Li. Experimental simulation study on pore clogging mechanism of porous pavement. *Construction and Building Materials*, Vol. 187, 2018, pp. 803-818.

[13] Chen, L. M., J. W. Chen, T. Lecher, T. H. Chen, and P. Davidson. Assessment of clogging of permeable pavements by measuring change in permeability. *Science of the Total Environment*, Vol. 749, 2020, pp. 141352.

[14] ASTM C 1701, Test method for infiltration rate of in place pervious concrete, ASTM International, West Conshohocken, Pennsylvania, United States, 2017.
[15] Manahiloh, K. N., B. Muhunthan, M. Kayhanian, and S. Y. Gebremariam. X-ray computed tomography and nondestructive evaluation of clogging in porous concrete field samples. *Journal of Materials in Civil Engineering*, Vol. 24, No. 8, 2012, pp. 1103-1109.
[16] Fwa, T. F., E. Lim, and K. H. Tan. Comparison of permeability and clogging characteristics of porous asphalt and pervious concrete pavement materials. *Transportation Research Record*, Vol. 2511, No. 1, 2015, pp. 72-80.
[17] Chen, J., H. Li, X. Huang, and J. Wu. Permeability loss of open-graded friction course mixtures due to deformation-related and particle-related clogging: Understanding from a laboratory investigation. *Journal of Materials in Civil Engineering*, Vol. 27, No. 11, 2015, pp. 04015023.
[18] Annan, A. P. Chapter 11: Ground-penetrating Radar. Near-surface Geophysics. Tulsa, Oklahoma: Society of Exploration Geophysicists, 2005, pp. 357-438.
[19] Daniels, D. J. (Ed.). Ground penetrating radar, Vol. 1, 2004.
[20] Wang, S., X. Sui, Z. Leng, J. Jiang, and G. Lu. Asphalt pavement density measurement using non-destructive testing methods: current practices, challenges, and future vision. *Construction and Building Materials*, Vol. 344, 2022, pp. 128154.
[21] Lai, W. W. L., X. Dérobert, and P. Annan. A review of Ground Penetrating Radar application in civil engineering: A 30-year journey from Locating and Testing to Imaging and Diagnosis. *Ndt & E International*, Vol. 96, 2018, pp. 58-78.
[22] Leng, Z., and I. L. Al-Qadi. Railroad ballast evaluation using ground-penetrating radar: laboratory investigation and field validation. *Transportation Research Record*, Vol. 2159, No. 1, 2010, pp. 110-117.
[23] Al-Qadi, I. L., W. Xie, D. L. Jones, and R. Roberts. Development of a time–frequency approach to quantify railroad ballast fouling condition using ultra-wide band ground-penetrating radar data. *International Journal of Pavement Engineering*, Vol. 11, No. 4, 2010, pp. 269-279.
[24] Roberts, R., I. L. Al-Qadi, E. Tutumluer, J. Boyle, and T. Sussmann. Advances in railroad ballast evaluation using 2 GHz horn antennas. *In Proc. 11th International Conference on Ground Penetrating Radar*, Columbus, OH., USA. 2006.
[25] Al-Qadi, I. L., S. Zhao, and P. Shangguan. Railway ballast fouling detection using GPR data: Introducing a combined time-frequency and discrete wavelet techniques. *Near Surface Geophysics*, Vol. 14, No. 2, 2016, pp. 145-153.
[26] Shangguan, P., I. L. Al-Qadi, and Z. Leng. Ground-penetrating radar data to develop wavelet technique for quantifying railroad ballast–fouling conditions. *Transportation Research Record*, Vol. 2289, No. 1, 2012, pp. 95-102.
[27] Oppenheim, A. V., R. W. Schafer, and J. R. Buck. Discrete-Time Signal-Processing. Pearson Prentice-Hall, Englewood Cliffs, N.J., 2005.
[28] AASHTO, T 269, Standard method of test for percent air voids in compacted dense and open asphalt mixtures, 2014.
[29] ASTM, D2041, Standard test method for theoretical maximum specific gravity and density of bituminous paving mixtures, West Conshohocken, P.A., 2003.
[30] Li, B., P. Zhang, X. Zhu, D. Wei, and Q. Li. Permeability model and characteristics analysis of porous asphalt mixture under the circulation clogging and cleaning. *Road Materials and Pavement Design*, 2022, pp. 1-21.
[31] Kayhanian, M., C. Suverkropp, A. Ruby, and K. Tsay. Characterization and prediction of highway runoff constituent event mean concentration. Journal of environmental management, Vol. 85, No. 2, 2007, pp. 279-295.
[32] Fernandes, F. M., and J. C. Pais. Laboratory observation of cracks in road pavements with GPR. *Construction and Building Materials*, Vol. 154, 2017, pp. 1130-1138.
[33] BS EN 12697-19:2012, Bituminous mixtures – Test method for hot mix asphalt-Part 19: Permeability of specimen, 2012.

[34] Davis, J. L., and A. P. Annan. Ground-penetrating radar for high resolution mapping of soil and rock stratigraphy. *Geophysical prospecting*, Vol. 37, No. 5, 1989, pp. 531-551.
[35] Wang, S., S. Zhao, and I. L. Al-Qadi. Real-time monitoring of asphalt concrete pavement density during construction using ground penetrating radar: theory to practice. *Transportation Research Record*, Vol. 2673, No. 5, 2019, pp. 329-338.
[36] Wang, S., S. Zhao, and I. L. Al-Qadi. Real-time density and thickness estimation of thin asphalt pavement overlay during compaction using ground penetrating radar data. *Surveys in Geophysics*, Vol. 41, No. 3, 2020, pp. 431-445.
[37] Al-Qadi, I. L., Q. Cao, L. Abufares, S. Wang, Ali, U. Mohamed and G. Renshaw. Moisture Content and In-place Density of Cold-Recycling Treatments. Illinois Center for Transportation/Illinois Department of Transportation, 2022.
[38] Maser, K., and T. Scullion. Automatic pavement subsurface profiling using radar: case studies of four experimental field sites. *Transportation Research Record*, Vol. 1344, 1992, pp. 148-154.
[39] Pérez-Gracia, V., D. Di Capua, R. González-Drigo, and L. Pujades. Laboratory characterization of a GPR antenna for high-resolution testing: Radiation pattern and vertical resolution. *NDT & E International*, Vol. 42, No. 4, 2009, pp. 336-344.
[40] Solla, M., S. Lagüela, H. González-Jorge, and P. Arias. Approach to identify cracking in asphalt pavement using GPR and infrared thermographic methods: Preliminary findings. *Ndt & E International*, Vol. 62, 2014, pp. 55-65.